Drug Design, Development and Therapy

Dovepress
Taylor & Francis Group

Open Access Full Text Article

ORIGINAL RESEARCH

Therapeutic Efficacy of Curcumin Nanoparticles in Parkinson's Disease: An Integrated Analysis of Network Pharmacology, Experimental Validation, and Gut Microbiota

Runhong Mu[1,*], Tengda Liu[1,*], Yu Zhang[1], Kexin Xiu[1], Xiao Guo[2], Wei Xia[3]

[1]School of Basic Medical Sciences, Beihua University, Jilin, Jilin, 132013, People's Republic of China; [2]School of Pharmacy, Beihua University, Jilin, Jilin, 132013, People's Republic of China; [3]School of Medical Technology, Beihua University, Jilin, Jilin, 132013, People's Republic of China

*These authors contributed equally to this work

Correspondence: Xiao Guo, School of Pharmacy, Beihua University, Jilin, Jilin, 132013, People's Republic of China, Email guoxiao@beihua.edu.cn; Wei Xia, School of Medical Technology, Beihua University, Jilin, Jilin, 132013, People's Republic of China, Email 496966717@qq.com

Background: Parkinson's disease (PD) ranks as the second most common neurodegenerative condition globally, with a rising occurrence alongside the aging demographic. Previous studies have demonstrated that curcumin monomers can alleviate PD symptoms and slow disease progression, whereas nano-drug delivery systems significantly improve their bioavailability. Notably, gut microbiota imbalance significantly contributes to the onset and advancement of PD; however, the mechanisms by which curcumin nanoparticles produce their therapeutic impact on PD are not yet well understood.

Materials and Methods: Initially, network pharmacology was tapped to forecast the probable targets and signaling routes for curcumin in combating Parkinson's Disease. Later on, molecular docking techniques and molecular dynamics experiments were utilized to substantiate its binding effectiveness. Curcumin nanoparticles were synthesized via the emulsion-solvent evaporation technique. After establishing PD models, multidimensional validation was performed using behavioral experiments, serological assays, Western blotting, hematoxylin–eosin staining, and 16S ribosomal RNA (16S rRNA) sequencing.

Results: Network pharmacology analysis revealed that curcumin acts through multiple targets and pathways. In vivo experiments demonstrated that curcumin nanoparticles enhanced motor capabilities in Parkinson's disease mice, bolstered antioxidant enzyme levels, alleviated oxidative stress, and inhibited neuronal apoptosis via the Akt signaling pathway. Histopathological analysis showed significant improvements in the number and arrangement of neurons in the hippocampal dentate gyrus (DG) region. Furthermore, remodeling of the gut microbiota and metabolic regulation alleviated neuroinflammation and enhanced neuroprotection.

Conclusion: Curcumin nanoparticles inhibit neuronal apoptosis by activating the Akt signaling pathway and, while also remodeling the gut microbiota microenvironment, collectively ameliorate PD pathology. This study provides pharmacological evidence that curcumin nanoparticle therapy mediates its therapeutic actions through multiple mechanisms, and identifies potential therapeutic targets for PD treatment.

Keywords: network pharmacology, curcumin nanoparticles, parkinson's disease, gut microbiota

Introduction

The accelerating demographic shift toward an aging population globally has precipitated a marked rise in Parkinson's disease (PD) incidence. According to World Health Organization (WHO) epidemiological reports, PD currently affects over 8.5 million individuals worldwide, of whom 5.8 million are disabled and approximately 329,000 die annually as a result of the disease. PD severely impairs the health of the elderly, and the resulting functional disabilities substantially increase medical demands and thereby imposing considerable economic strain on international health infrastructures.[1]

https://doi.org/10.2147/DDDT.S566113
Received: 6 October 2025
Accepted: 9 January 2026
Published: 22 January 2026

Graphical Abstract

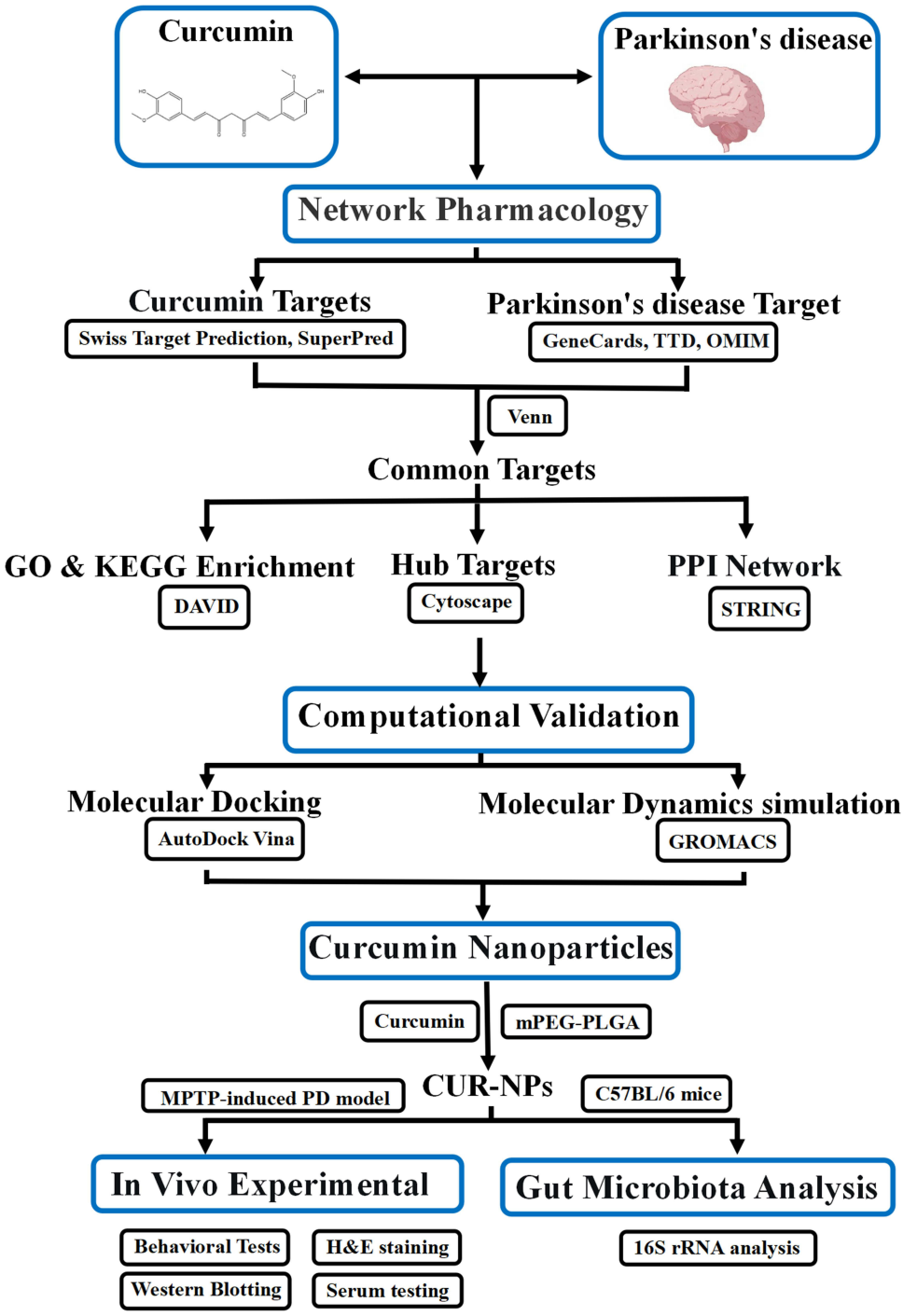

PD fundamentally arises from the gradual deterioration of dopamine-producing neural cells within the midbrain's nigral region, accompanied by the aggregation of alpha-synuclein-rich inclusions. Symptomatically, this neurodegenerative disorder presents cardinal motor deficits including bradykinesia and involuntary shaking during inactivity, supplemented by diverse neuropsychiatric manifestations such as deteriorating executive functions, which collectively result in

deficits in speech and motor abilities.[2] At present, PD lacks curative therapies; disease management centers on pharmacological approaches with the dopamine precursor levodopa as the cornerstone intervention, surgical intervention, and rehabilitation to alleviate symptoms and slow disease progression. However, access to these treatments varies considerably, presenting particular challenges within economies classified as low to middle income.

Levodopa, the primary medication for PD, frequently induces adverse effects such as dyskinesia during its metabolism.[3] Consequently, creating novel therapeutics derived from natural sources that demonstrate efficacy alongside favorable safety profiles represents a crucial clinical objective. Curcumin (CUR), the principal active compound extracted from the rhizome of turmeric (comprising approximately 2%–6%, with a higher concentration in the root than in the stem), is an orange-yellow crystalline powder that is poor solubility in aqueous media but high solubility in ethanolic solutions, propylene glycol, as well as dichloromethane. Traditional Chinese Medicinal ingredients demonstrate significant advantages in disease treatment. Applications such as Tanshinone IIA demonstrates therapeutic activity against colorectal cancer,[4] Celastrol alleviates liver fibrosis by inducing ferroptosis in hepatic stellate cells,[5] and Aloin aids in the management of chronic prostatitis/chronic pelvic pain syndrome,[6] all underscore the vital value of these active constituents within modern medicine. CUR, a key active component in Traditional Chinese Medicine (TCM), has garnered extensive attention for its diverse pharmacological activities in anti-inflammatory, antioxidant, and anti-tumour domains.[7] Toxicological studies have demonstrated a favorable safety profile for curcumin at high oral doses,[8] and it has been approved as a food additive by the WHO, FAO, and FDA. Previous clinical evidence has indicated that the Akt signaling activation is a key mechanism for neuroprotection in Parkinson's disease.[9] Given its poor water solubility, curcumin nanoparticles were prepared in this study using the emulsion–solvent evaporation method to construct a nanodrug delivery system aimed at enhancing solubility and bioavailability.

Network pharmacology has emerged as an indispensable discipline for advancing traditional Chinese medicine.[10] By constructing a multidimensional network that links active components, targets, and diseases, this approach systematically elucidates the molecular mechanisms underlying herbal treatments, thereby facilitating a comprehensive understanding of their overall pharmacological effects. This research integrates Systems pharmacology network analysis, molecular docking (AutoDock Vina), molecular dynamics simulations (100ns), and complemented by experimental validation to confirm curcumin's molecular targets and binding activities, providing empirical evidence to optimize clinical therapies.

The brain and gut microbiota interact bidirectionally through the brain-gut axis.[11] Gut microbiome not only regulates host emotions, including anxiety and depression, as well as cognitive functions, but also releases inflammatory mediators that can induce neuroinflammation, thereby driving PD pathogenesis and progression.[12] PD patients commonly exhibit reduced gut microbiota abundance and diversity, accompanied by gastrointestinal non-motor symptoms such as constipation.[13] Restoring gut microecological balance may help delay the pathological progression of PD.[14] Clinical 16S rRNA sequencing has revealed PD-specific gut dysbiosis, notably a reduction in Prevotellaceae and an increase in Enterobacteriaceae linked to motor symptoms.[15] Therefore, employing 16S rRNA sequencing to dynamically analyze changes in gut microbiota during PD progression dynamics may establish a mechanistic foundation for pioneering disease-modifying therapies.

Nevertheless, a critical gap persists in developing integrated therapeutic strategies that systemically regulate the gut-brain axis in Parkinson's disease while overcoming the poor bioavailability of natural curcumin.[16] Although the neuroprotective role of the Akt pathway is well established[17] and gut dysbiosis is recognized as a core pathological driver,[18,19] whether a nanoformulated curcumin can simultaneously modulate both systems remains unexplored. To address this, we developed novel mPEG-PLGA-based curcumin nanoparticles (CUR-NPs)—a nanodelivery system designed to enhance brain delivery.[20] This study aims to systematically evaluate the neuroprotective effects of CUR-NPs through synergistic activation of the Akt signaling pathway and remodeling of gut microbiota, using an integrated approach combining network pharmacology, molecular dynamics simulations, experimental validation, and 16S rRNA sequencing.

Materials and Methods

Chemicals and Reagents

Curcumin (CAS No. 458–37-7) was sourced from Beijing Solarbio Science & Technology Co., Ltd. (Beijing, China) in a 5 g container (Catalog No. C7090, Lot No. 2230818001) with ≥95.0% purity; 1-Methyl-4-Phenyl-1,2,3,6-Tetrahydropyridine (MPTP, Shanghai yuanye Bio-Technology Co., Ltd) Dichloromethane, Sodium cholate, Dimethyl sulfoxide (DMSO) (Shanghai Macklin Biochemical Technology Co., Ltd., Shanghai, China); Akt, p-Akt (Biodragon (Suzhou) Biotechnology Co., Ltd., Suzhou, China); GAPDH (Servicebio Technology Co., Ltd., Wuhan, China); Glutathione peroxidase (GSH-Px) and Catalase (CAT) Assay Kits (Nanjing Jiancheng Bioengineering Institute, Nanjing, China); Reduced Glutathione (GSH) and Bicinchoninic Acid (BCA) Protein Assay Kits (Beyotime Biotechnology, Shanghai, China); Hematoxylin and Eosin (H&E) Staining Kit (Beijing Leagene Biotech Co., Ltd., Beijing, China).

Animals and Groups

Forty male C57BL/6 mice, aged 5–6 weeks and weighing approximately 20 grams, were obtained from Liaoning Changsheng Biotechnology Co., Ltd. (Liaoning, China).

Forty male C57BL/6 mice (weight averaging 20 ± 2 g; aged 6 weeks) were randomly allocated to five distinct groups (with 8 mice in each): Control, MPTP model, MPTP + CUR, MPTP + CUR-NPs, and MPTP + Madopar (positive control). Except for the control group, we gave all the mice daily intraperitoneal injections of MPTP (1-methyl-4-phenyl-1,2,3,6-tetrahydropyridine) at a dose of 30 mg per kg for a solid week. The control group got the same amount of saline instead. The treatment groups received either intravenous (i.v.) tail vein injections of CUR (200 mg/kg/day x 7) or CUR-NPs (200 mg/kg/day x 7), or oral gavage of Madopar (125 mg/kg/day x 7). The control and MPTP model groups were administered saline injections.

Ethical clearance for this investigation was formally granted during August 2024 by the Laboratory Animal Ethics Committee at Beihua University (Approval No. 2024082117). All procedures involving laboratory animals were conducted in full compliance with globally established ethical guidelines governing biomedical research, specifically adhering to the American Veterinary Medical Association (AVMA) Guidelines for the Euthanasia of Animals.

At the end of the experiment, all mice were humanely euthanized. Euthanasia was performed by cervical dislocation under deep anesthesia induced with an overdose of sodium pentobarbital (150 mg/kg, i.p). Death was confirmed by the absence of respiration and heartbeat. We implemented rigorous protocols to actively safeguard animal welfare, systematically reducing discomfort and distress throughout experimental phases. The animal housing environment complied with international guidelines.

Network Pharmacology

The canonical SMILES representation of curcumin was acquired from PubChem (https://pubchem.ncbi.nlm.nih.gov). Subsequent target prediction for this compound was conducted via the SwissTargetPrediction platform (http://swisstargetprediction.ch/) and the SuperPred (https://prediction.charite.de/subpages/target_prediction.php), identifying potential therapeutic targets, with a probability threshold set at >0 for screening.

Relevant targets for Parkinson's disease were identified through keyword searches in integrated databases including GeneCards database (https://www.genecards.org/), the Therapeutic Target Database (TTD, https://db.idrblab.net/ttd/), and the Online Mendelian Inheritance in Man (OMIM) database (https://www.omim.org/). Relevant disease targets were compiled from the search results of these databases.

Common therapeutic targets between curcumin and Parkinson's disease were systematically determined utilizing an interactive Venn diagram platform, revealing potential shared pathogenic mechanisms (https://bioinformatics.psb.ugent.be/webtools/Venn/).

To start, we fed a list of likely suspects into the STRING database (https://cn.string-db.org), making sure to specify "Homo sapiens". The resulting protein interaction data, which we snagged in TSV format, was then imported into Cytoscape (version 3.9.1). That's where we built and picked apart the protein-protein interaction network.

The DAVID platform (https://david.ncifcrf.gov/) facilitated functional annotation for pivotal common targets, using Homo sapiens as the reference species. The acquired GO terms and KEGG pathways were graphically rendered using the bioinformatics online interface (https://www.bioinformatics.com.cn/).

The interaction network of "CUR-Common Targets-PD" was generated employing Cytoscape (version 3.9.1) software. The network primarily consists of nodes (representing entities) and edges (representing interactions). The key network targets were determined through topological analysis employing Cytoscape's integrated plugins cytoHubba and MCODE.

Molecular Docking

The structures of the core protein targets in crystal form were obtained from the RCSB database (https://www.rcsb.org/). Curcumin's two-dimensional (2D) and three-dimensional (3D) structure was sourced from PubChem. The curcumin's structural data were acquired through the PubChem database. Protein structures were prepared using PyMOL software (version 3.0.4) by removing water molecules and co-crystallized ligands. The curcumin structure was prepared for molecular docking using AutoDock Vina (version 1.5.7) by adding hydrogen atoms and assigning Gasteiger charges. Molecular docking were carried out with the aid of AutoDock Vina to determine the strength of the interactions between curcumin and the specified proteins. The conformations displaying the weakest binding energies were then chosen and depicted graphically using PyMOL software.

Molecular Dynamics Simulation

To assess curcumin-AKT1 binding strength, Molecular Dynamics simulations (MD simulations) were executed. The curcumin–AKT1 complex underwent a 100 ns MD simulations using GROMACS (version 2020.6). Amber99SB force field utilized for protein structure. The ligand topology file for curcumin was generated based on the General Amber Force Field 2 (GAFF2) parameters. The system was housed in a cubical simulation box with a periodic boundary of 1.2 nm. We used the SPC water model for the setup. To balance the system's charge, we introduced sodium and chloride ions using the Monte Carlo technique. We then fine-tuned the energy with the steepest descent method. Afterward, we allowed the system to reach equilibrium within the NVT (constant particle count, volume, and temperature) and NPT (constant particle count, pressure, and temperature) conditions for 100,000 steps, each lasting 100 picoseconds. This was all coupled with a time step of 0.1 picoseconds. In the end, we ran a 100-nanosecond production simulation at a steady state of 310 Kelvin and 1 atmosphere of pressure.

Curcumin Nanoparticles Preparation

Curcumin-loaded nanoparticles (CUR-NPs) were synthesized via the emulsion-solvent evaporation method. Briefly, curcumin was dissolved in dimethyl sulfoxide (DMSO), while mPEG-PLGA was dissolved in dichloromethane. The two solutions were vortexed separately and subsequently combined. The resulting mixture was sonicated at 25% amplitude for 5 minutes to form a primary emulsion. An aqueous solution of sodium cholate (2% w/v) was then added, followed by sonication at 30% amplitude for 10 minutes. This emulsion was subsequently added dropwise into a 0.6% (w/v) sodium cholate solution under magnetic stirring at 500–1000 rpm. Organic solvents were removed by rotary evaporation at 50°C. The resulting suspension was centrifuged at 12,000 rpm for 10 minutes, and the process was repeated three times with resuspension in deionized water to collect and purify the nanoparticles. The pellet was washed twice with deionized water to obtain the purified CUR-NPs.

The particle size and polydispersity index (PDI), and zeta potential of CUR-NPs were determined using a Malvern Zetasizer Nano analyzer, while nanoparticle morphology was determined through TEM.

In vivo Experiments

Behavioral Tests

Following the treatment period, behavioral assessments were conducted, Incorporating the Morris water maze, open field test, and spontaneous activity evaluation. The Morris water maze test was conducted in a circular pool (120 cm in diameter). The open field test was performed by placing each mouse in the center of a custom-made testing field (50 cm × 50 cm × 40 cm) for a 5-min free exploration to evaluate exploratory behavior. Spontaneous activity was

assessed simultaneously for all mice in a dedicated apparatus featuring six separate testing arenas (14 cm × 11 cm × 11 cm each).

Serum Oxidative Stress Indicators

Serum was extracted from blood draws. Serum levels of GSH-Px, reduced GSH, and CAT were assessed with commercial test kits following the producers' guidelines.

Western Blotting Analysis

We extracted proteins from the brain tissue and measured them using the BCA protein assay kit. We then ran the equal quantities of protein through an SDS-PAGE and moved them onto PVDF membranes. These membranes were treated with a 5% skim milk block for two hours at room temp before being incubated overnight at 4 degrees with primary antibodies for tyrosine hydroxylase, phospho-Akt, Akt, and GAPDH. Membranes were exposed to suitable HRP-linked secondary antibodies and incubated for 2 hours at ambient temperature post-washing. Protein bands were visualized using an enhanced chemiluminescence (ECL) detection kit. For Western blot quantification, band intensities were measured with ImageJ software and normalized to GAPDH. Western blot supplementary materials are shown in Supplementary Figures S1–S4.

Histopathological Examination

Deparaffinized brain sections underwent xylene treatment, subsequent rehydration via graded ethanol, and hematoxylin and eosin staining, with hematoxylin applied for 5 minutes followed by eosin counterstaining for 60 seconds. Samples underwent serial ethanol dehydration, xylene washes, and were finally sealed using neutral balsam. Neuronal morphology was examined and imaged using an Olympus light microscope.

Gut Microbiota Analysis

We gathered fecal samples from the Control, MPTP, CUR-NPs, and Madopar groups. Each sample was immediately flash-frozen and then deep-stored at −80°C. To explore the potential link between the gut's microbial makeup and Parkinson's disease, we tapped LC-Bio Technology Co., Ltd. (Hangzhou, China) to perform 16S rRNA gene sequencing analysis on the gut microbiota.

Statistical Analysis

Statistical analysis was performed using OriginPro 2025. The sample sizes (n = 5 or 6) represent independent biological replicates. Data are presented as the mean ± standard deviation (SD). Group differences in animal experiments were analyzed by one-way analysis of variance (ANOVA), followed by Tukey's honest significant difference (HSD) test for post-hoc pairwise comparisons. A P value of less than 0.05 was considered statistically significant. (*P<0.05).

Results

Network Pharmacological Analysis of Curcumin for PD Treatment

CUR's SMILES notation, obtained from PubChem, was then utilized by SwissTargetPrediction and SuperPred. After removing redundant entries, a total of 67 CUR targets were identified (Figure 1A). Searching the GeneCards, TTD, and OMIM databases yielded 10,537 PD-related targets. Using an online Venn diagram tool, 56 common targets at the intersection of CUR and PD were identified (Figure 1B). These typical Homo sapiens-specific targets were inputted into the STRING database for constructing a protein interaction network and producing a TSV file. Cytoscape software (v3.9.1) was employed to visualize the PPI network (Figure 1B), which comprised 52 nodes and 215 edges. The top 10 targets were identified using the Degree, EPC, MNC, and MCC algorithms implemented in the cytoHubba plugin. The core targets underlying curcumin's potential efficacy against PD were identified as AKT1, STAT3, BCL2, EGFR, GSK3B, EP300, APP, and CDK2 (Figure 1C). Topological analysis revealed AKT1 as the most central node, prompting our focused investigation on the Akt signaling pathway in the following experimental validation. Analysis using the

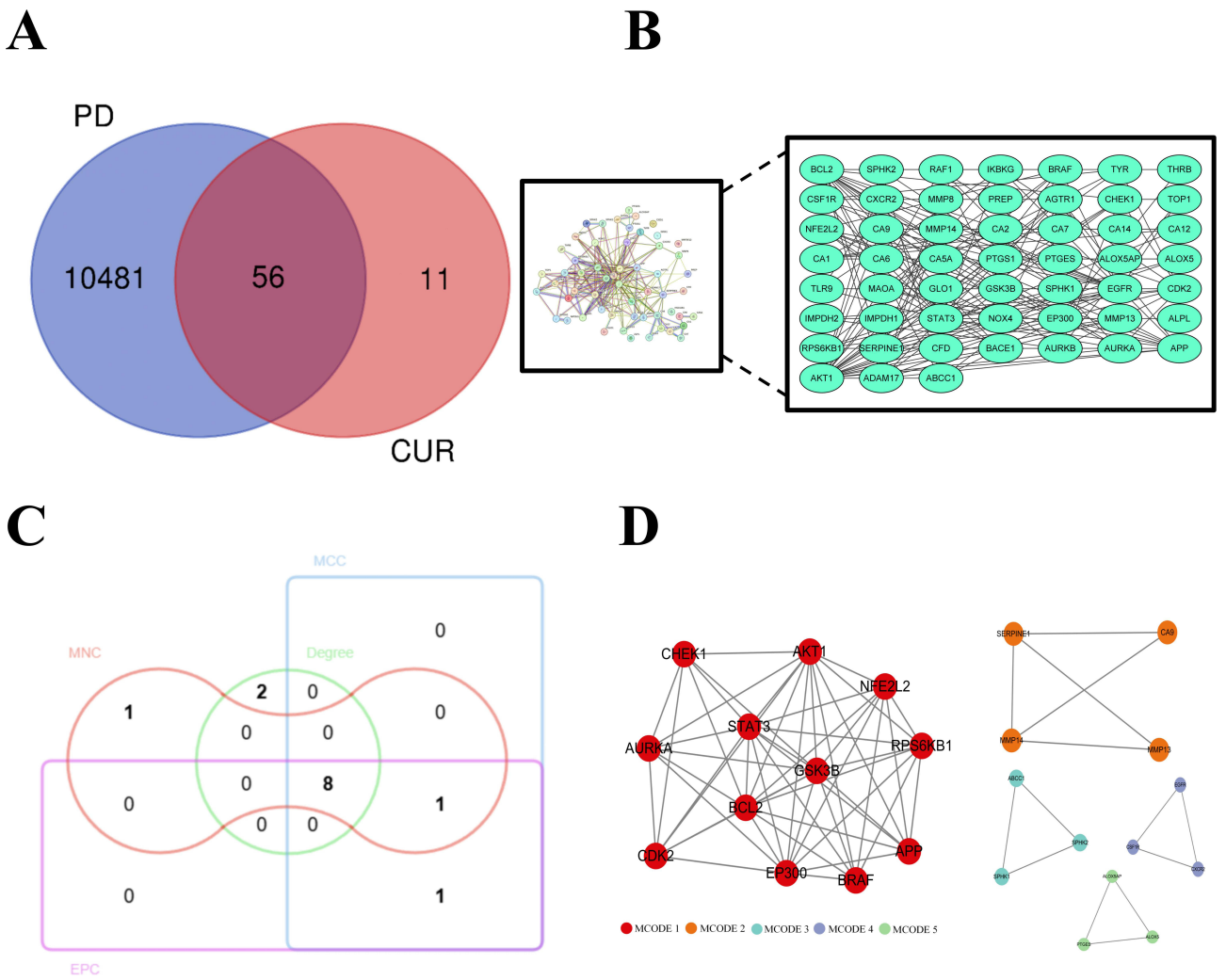

Figure 1 Network Pharmacology Analysis of Venn and PPI: (**A**) Venn diagram of overlapping targets between CUR and PD; (**B**) Protein-protein interaction (PPI) network; (**C**) Venn diagram of core overlapping targets between CUR and PD; (**D**) MCODE analysis.

MCODE plugin revealed five PPI network clusters (Figure 1D), with seven of the eight core targets (excluding EGFR) located within the primary cluster (MCODE1).

The primary objectives were incorporated into the DAVID database, resulting in the identification of 147 GO terms. These comprised 84 Biological Process (BP) terms, Primarily linked to the inhibition of autophagy and suppression of gene expression, peptide-serine phosphorylation, learning and memory, and circadian rhythm; 17 Cellular Component (CC) terms, primarily related to the cytoplasm, nucleus, protein complexes, and postsynaptic structures; and 46 Molecular Function (MF) terms, encompassing protein kinase interaction, homodimerization, kinase function, and transcription factor recruitment. Figure 2A presents the visualization of the top five enriched terms, as generated by the online bioinformatics platform.

Key targets showed marked enrichment across 67 KEGG pathways (Figure 2B). Key pathways included the Akt-associated signaling pathways (such as PI3K-Akt, HIF-1, and FoxO,signaling pathways), as well as the growth hormone synthesis and secretion pathway.

Upon examining the KEGG data, we created a "Drug-Disease-Target-Pathway" interaction network utilizing Cytoscape, as seen in Figure 3. This visual depiction clearly shows that CUR impacts Parkinson's Disease positively by working in tandem on various targets and pathways.

https://doi.org/10.2147/DDDT.S566113

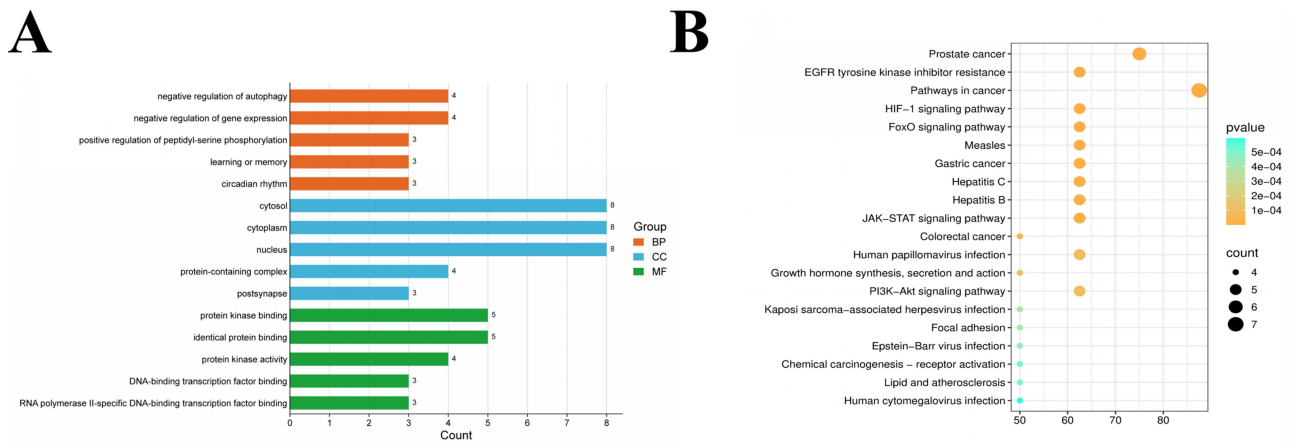

Figure 2 Network Pharmacology Analysis of GO and KEGG: (**A**) GO enrichment analysis; (**B**) KEGG pathway enrichment analysis.

Molecular Docking Analysis

Molecular docking binding energy thresholds were defined as follows: < −4.25 kcal/mol (binding potency), < −5.0 kcal/mol (adequate efficacy), and < −7.0 kcal/mol (significant efficacy). As shown in Figure 4A–H, The CUR-target complexes, including AKT1, BCL2, and others, exhibited binding energies below −5.0 kcal/mol (Figure 4I), confirming its strong binding affinity.

Molecular Dynamics Simulation

The root mean square deviation (RMSD) is a reliable measure of how well a protein and its ligand hold together; essentially, it tells you how much the atoms move from their starting positions. A smaller RMSD generally suggests a more stable structure. Throughout our simulation, the CUR-AKT1 complex displayed remarkable stability, with RMSD values hovering around 0.15 nm (Figure 5A), which points to a strong, stable binding interaction. Root mean square fluctuation (RMSF), on the other hand, gives us an idea of how wobbly individual amino acids are within the protein. The relatively low RMSF values we observed (Figure 5B) suggest that the amino acid residues were not moving around much, further reinforcing the complex's overall structural integrity. We also saw that the number of hydrogen bonds linking the ligand and protein fluctuated between 0 and 4, averaging out at 3 (Figure 5C), suggesting strong hydrogen bonding interactions. Upon closer inspection, the radius of gyration (Rg) and solvent-accessible surface area (SASA) remained fairly stable throughout the simulation (Figure 5D and E). This suggests that the protein did not undergo any major conformational shifts when the ligand latched on. Hydrogen bonds are critical in ligand–protein interactions. The CUR-AKT1 complex exhibited stable binding characteristics, with consistent hydrogen bond formation and minimal structural fluctuations throughout the simulation period. While these computational findings suggest favorable binding interactions, further experimental validation is required to confirm target specificity and assess potential off-target effects.

Preparation and Characterization of Curcumin Nanoparticles

As illustrated in Figure 6A, CUR-NPs were synthesized using mPEG-PLGA as the carrier through the emulsion-solvent evaporation method and subsequently characterized. The prepared CUR-NPs (Figure 6B) exhibited uniform spherical morphology under transmission electron microscopy (TEM)(Figure 6C), uniform particle size distribution, mean diameter 149.4 ± 87.57 nm, Zeta potential was −30.8 mV (Figure 6D and E).

Evaluating CUR-NPs' Impact on PD Mice's Motor Skills

After model establishment, mice underwent treatment. Post-treatment behavioral assessments (Figure 7A), encompassing the Morris water maze and open field tests, and spontaneous locomotor activity tests, assessed intergroup variance within murine models of MPTP-induced PD model mice. Drug dosages were adjusted according to body weight, and administration was recorded throughout the treatment period.

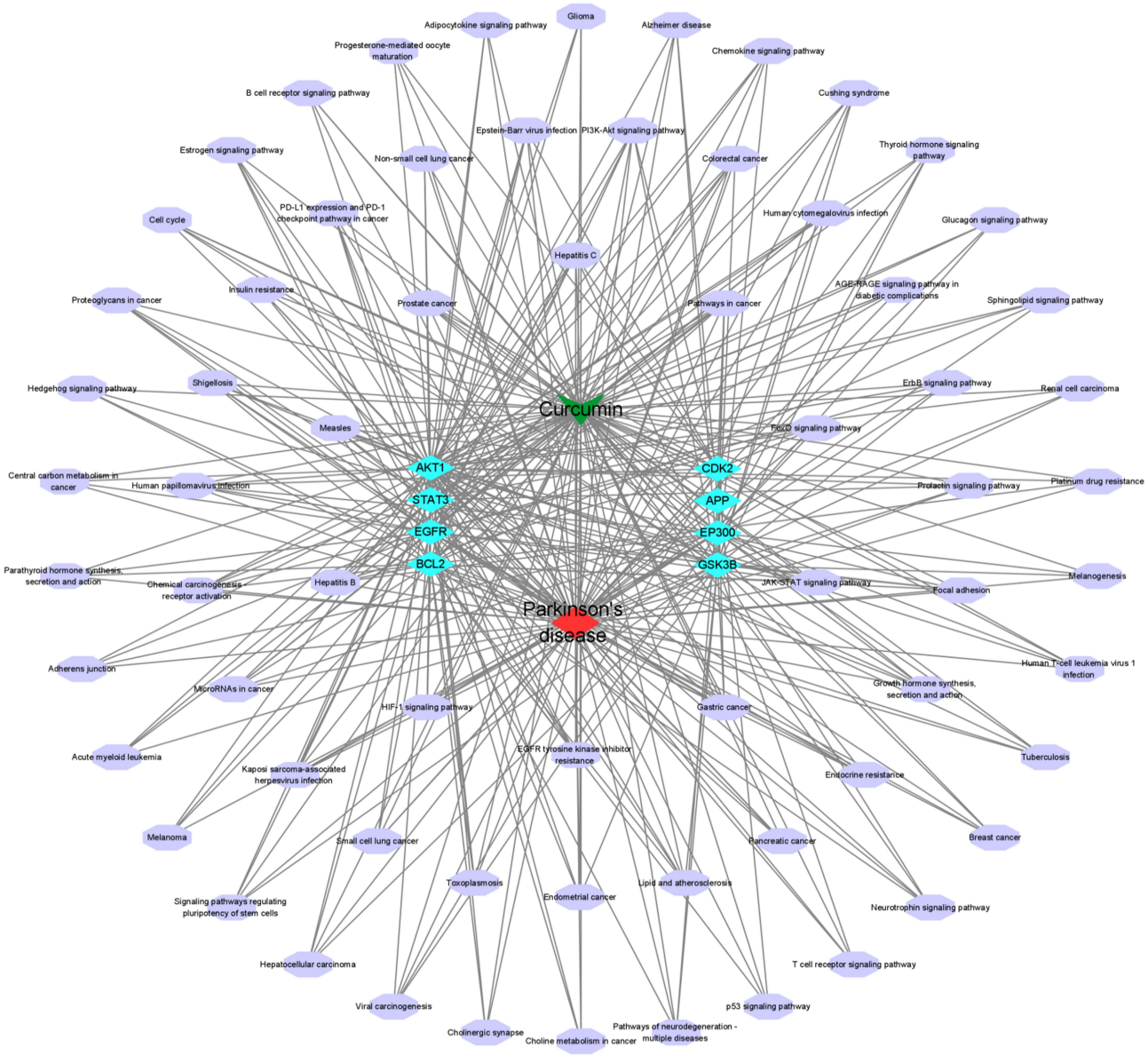

Figure 3 Network Pharmacology Analysis of Drug-Target-Pathway-Disease network.

Spontaneous Locomotor Activity Results

Locomotor activity was assessed by quantifying the number of spontaneous movements. Figure 7B reveals that controls displayed peak movement levels, exceeding the MPTP group's ($P < 0.001$). The MPTP group mice showed considerable decreases in overall locomotion and rearing activities. CUR-NPs treatment notably enhanced movement capabilities versus the MPTP group ($P < 0.001$), showcasing a higher efficacy than CUR alone. The Madopar-treated group also exhibited significant improvement ($P < 0.001$). No significant differences were observed between the CUR and Madopar groups relative to the CUR-NPs group.

Open-field test results (Figure 7C–F) revealed that compared with the control group, MPTP-exposed mice exhibited significantly reduced locomotor activity, active period duration, and central zone dwell time ($P < 0.001$). The CUR-NPs treatment group demonstrated significant improvements in all metrics relative to the MPTP group ($P < 0.001$), indicating marked motor function recovery. The Madopar group also exhibited a significant increase ($P < 0.001$). The CUR group demonstrated improvements over the MPTP group in total distance travelled ($P < 0.001$), time spent in the central area ($P < 0.001$), and total activity time ($P < 0.05$), though it differed significantly from the CUR-NPs group. Compared with the

https://doi.org/10.2147/DDDT.S566113

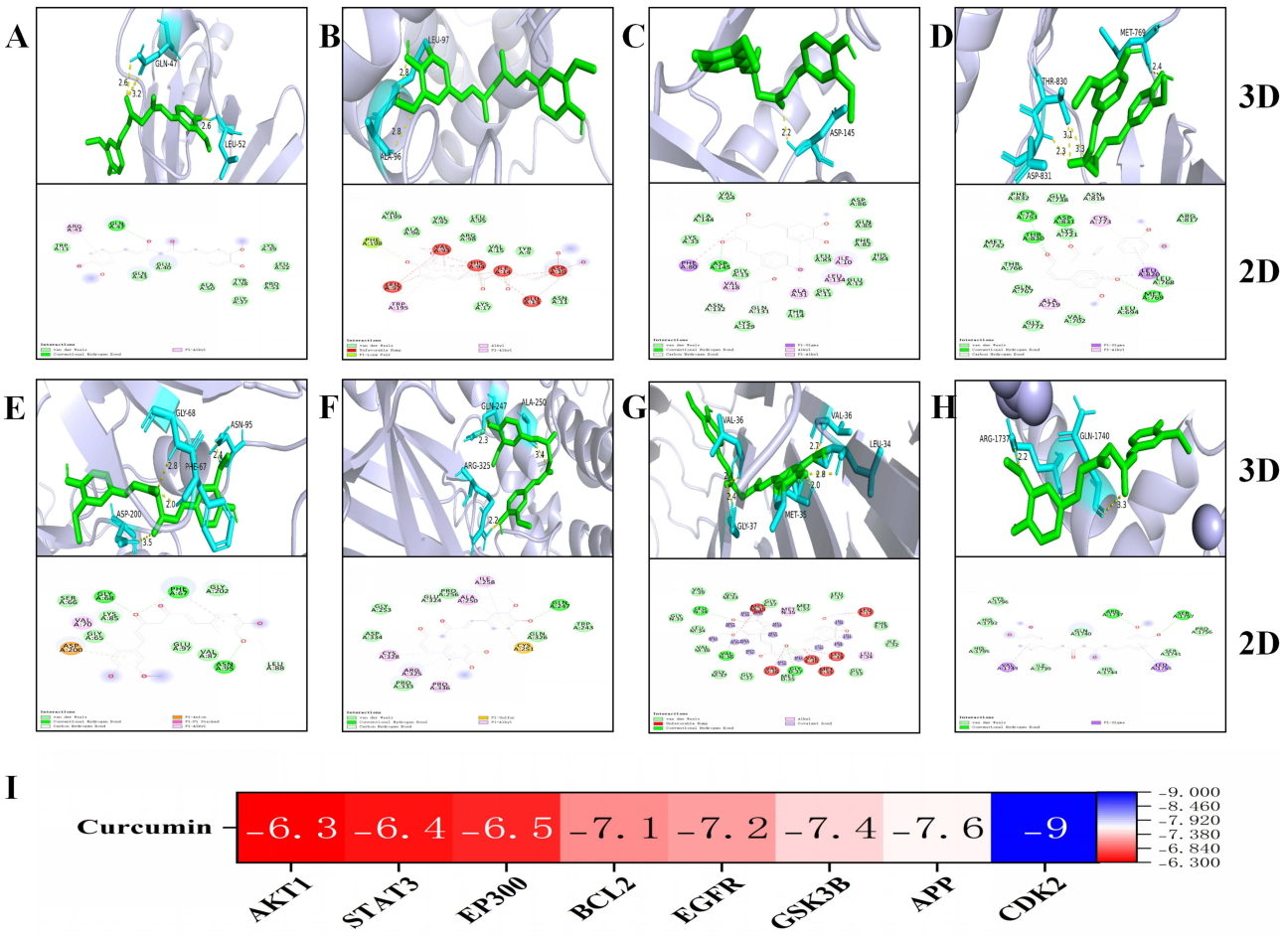

Figure 4 Molecular Docking of CUR Core Targets for Treating PD: (**A**) CUR-AKT1; (**B**) CUR-BCL2; (**C**) CUR-APP; (**D**) CUR-STAT3; (**E**) CUR-GSK3B; (**F**) CUR-CDK2; (**G**) CUR-EP300; (**H**) CUR-EGFR; (**I**) Binding energy thermogram of molecular docking.

CUR-NPs group, Madopar group mice exhibited significant differences in total distance travelled ($P < 0.05$) and overall activity duration ($P < 0.001$), while no significant difference was observed in central area dwell time. The CUR group showed significantly reduced overall activity duration ($P < 0.001$), central area dwell time, and total distance travelled ($P < 0.05$). These behavioral improvements correspond to improved motor function in MPTP-induced PD mice. The superior performance of CUR-NPs compared to free curcumin suggests enhanced bioactivity, possibly due to improved bioavailability of the nanoformulation.

Morris Water Maze Test Results

Mice in the MPTP group exhibited reduced exploratory behaviour and significantly prolonged immobility time ($P < 0.001$). The CUR-NPs treatment group demonstrated markedly superior performance compared to the MPTP group ($P < 0.001$), approaching the levels observed in the control group. The Madopar group yielded comparable results to the CUR-NPs group ($P < 0.001$), both significantly outperforming the CUR group ($P < 0.01$). The efficacy of the CUR group, measured by distance to the target area, was lower than that of the CUR-NPs group ($P < 0.001$); there was a significant difference in immobility time ($P < 0.01$). The Madopar group showed a difference in distance to the central area ($P < 0.01$) but no significant difference in immobility time.

Post-treatment, compared to the MPTP group, therapies increased spontaneous exploration distance and shortened immobility time, indicating that CUR-NPs improved motor function in MPTP-induced PD mice (Figure 8A–C). Therefore, the significant behavioral improvements confirm that the CUR-NPs mitigates motor dysfunction in PD mice, an effect attributable to its enhanced bioavailability and consequent neuroprotective efficacy.

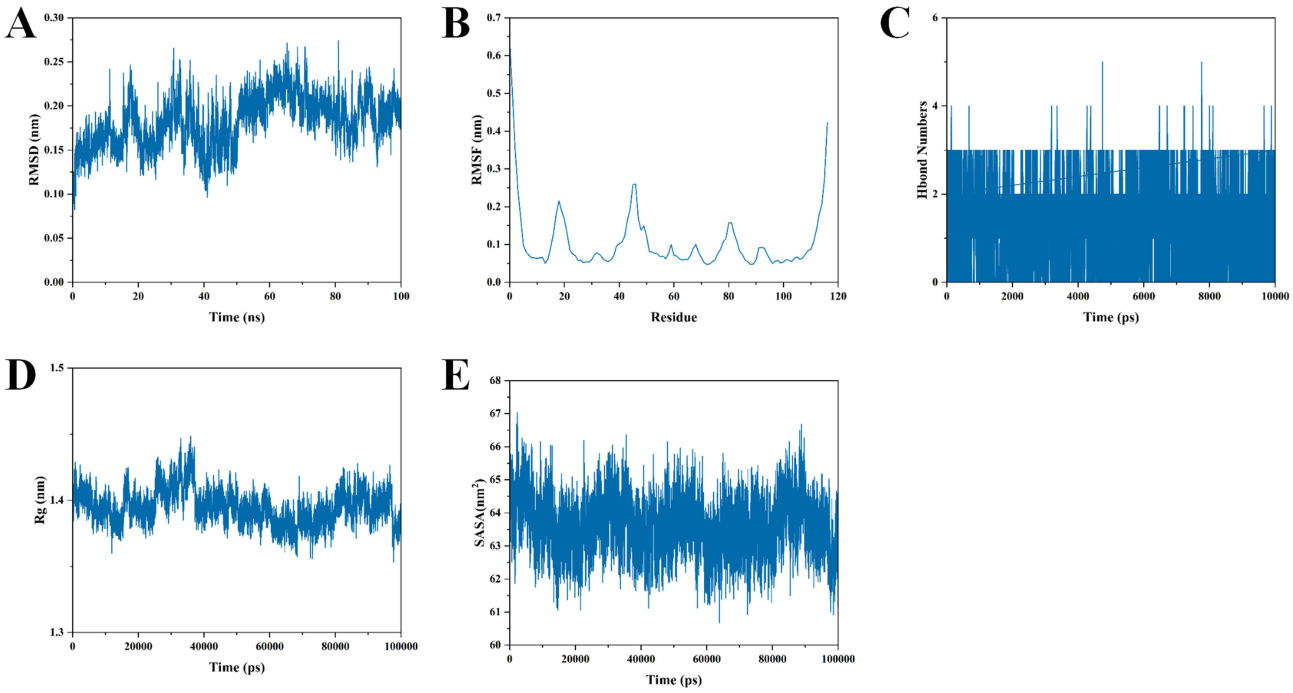

Figure 5 Molecular Dynamics Simulation of the CUR-AKT1 Complex: (**A**) Root-mean-square deviation (RMSD) plot; (**B**) Root-mean-square fluctuation (RMSF) plot; (**C**) Hydrogen bond (H-bond) count analysis; (**D**) Radius of gyration (Rg); (**E**) Solvent accessible surface area (SASA).

Impact of CUR-NPs on Antioxidant Enzymes in the Serum of PD Mice

Results (Figure 9A–C) indicated a substantial decrease in the serum catalase, glutathione, and glutathione peroxidase levels in the MPTP group relative to the Control group ($P < 0.001$). CUR-NPs treatment significantly increased serum CAT, GSH, and GSH-Px activities in PD mice compared to the MPTP group ($P < 0.001$). The CUR group exhibited significant differences in CAT activity ($P<0.05$), GSH activity ($P<0.001$), and GSH-Px activity ($P<0.01$) compared with the CUR-NPs group, whilst showing no significant differences in enzyme activity relative to the Madopar group. CUR-NPs may exert their therapeutic effect on PD by enhancing antioxidant enzyme activity and reducing oxidative stress levels.

Western Blotting Analysis of PD-Related Protein Levels

TH is closely associated with dopamine synthesis, and its dysfunction contributes to PD onset and progression. Figure 10A and B illustrates that TH levels in the MPTP group were notably lower than in the Control group ($P < 0.001$), indicating a significant decrease. On the other hand, CUR-NPs therapy notably elevated TH levels, particularly when contrasted with the MPTP group ($P < 0.001$). Notably, these levels were also substantially different from those observed in both the CUR group and the MPTP group ($P < 0.05$). Based on the predictions from network pharmacology that highlighted the centrality of AKT1, we assessed the activation of the Akt signaling pathway. Western blot analysis focusing on TH, p-AKT, and AKT levels. The data from the Western blot analysis, as depicted in Figure 11A and B, revealed a stark difference. The MPTP-induced group showed a marked decrease in the phosphorylation of AKT relative to the Control group, with the disparity being statistically significant ($P < 0.001$), suggesting a strong inhibition of the Akt signaling pathway. In the CUR-NPs group, mice showed a marked increase in Akt phosphorylation compared to the MPTP group ($P < 0.01$). Furthermore, the level was also significantly higher than that in the CUR group ($P < 0.05$). The upregulation of TH and Akt phosphorylation experimentally validates the central role of AKT1 in mediating neuroprotection, a key prediction from our network pharmacology analysis.

Hematoxylin and Eosin (H&E) Staining Analysis

The hippocampus' dentate gyrus (DG), crucial for memory and cognition, underwent histological analysis. Neuronal morphology was assessed using H&E staining (Figure 12A and B). The MPTP group displayed fewer neurons, structural

https://doi.org/10.2147/DDDT.S566113

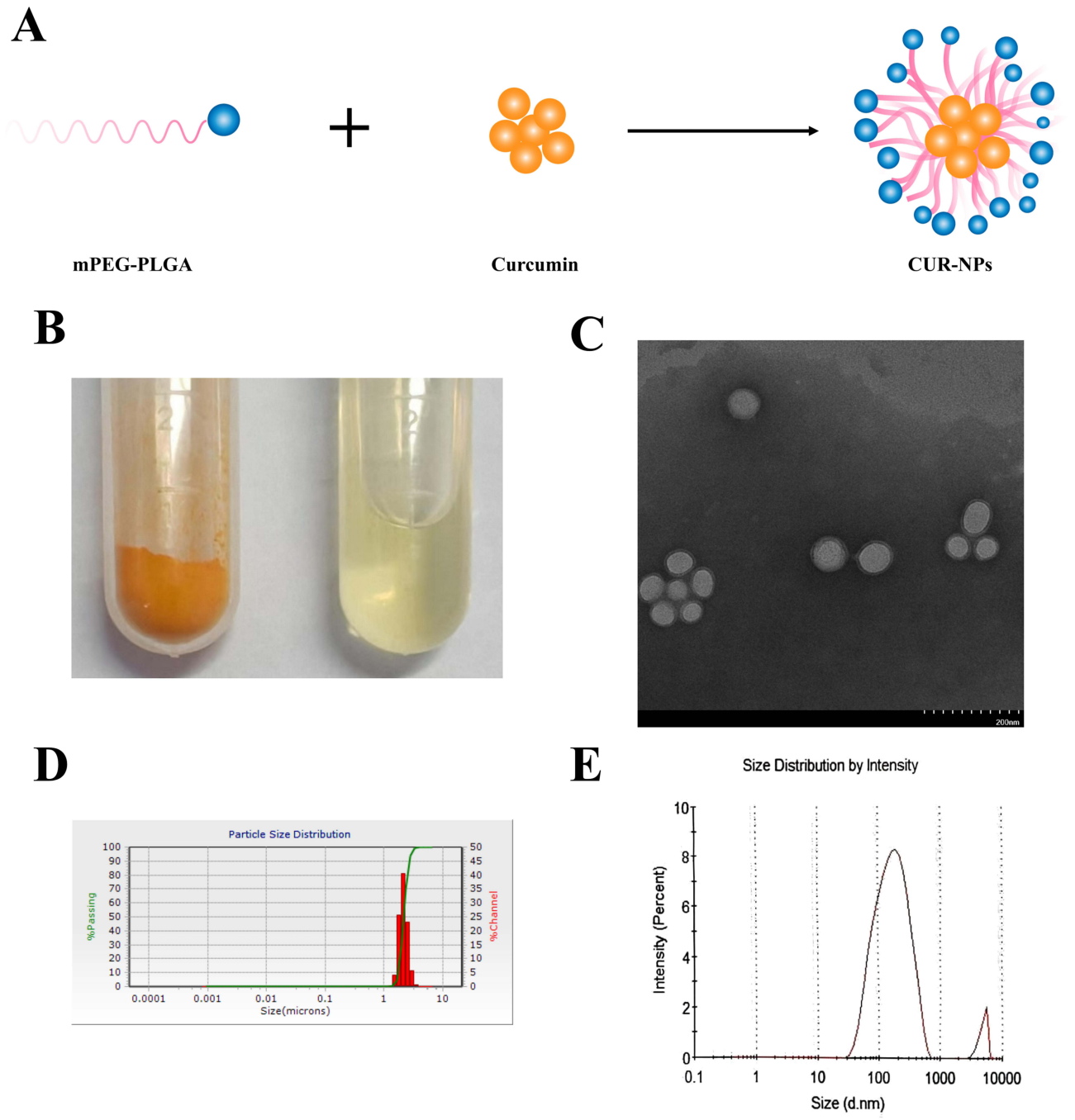

Figure 6 Synthesis and Characterization of CUR-NPs: (**A**) Schematic diagram of CUR-NPs synthesis; (**B**) free curcumin (left) and the synthesized CUR-NPs suspension (right); (**C**) Transmission electron microscopy (TEM) image of CUR-NPs; (**D**) Particle size distribution diagram of CUR-NPs; (**E**) Size distribution diagram of CUR-NPs.

disarray, indistinct cell boundaries, elevated nuclear condensation, and cytoplasmic vacuolization. Furthermore, Nissl body counts were reduced in the MPTP group, indicating severe neurotoxicity induced by MPTP. The Control group showed significantly better neuronal count and arrangement than the MPTP group. Both the CUR-NPs and Madopar (positive control) groups showed improvements in overall morphology, cellular arrangement, and Nissl body quantity. These observations indicate severe drug-induced damage in the hippocampal DG region of MPTP group mice, which was ameliorated in the treatment groups. Given that neuronal damage is often accompanied by apoptosis, combined with the Western blotting results, the results indicate that CUR-NPs could safeguard dopaminergic neurons by preventing neuronal apoptosis through the PI3K/Akt signaling pathway.

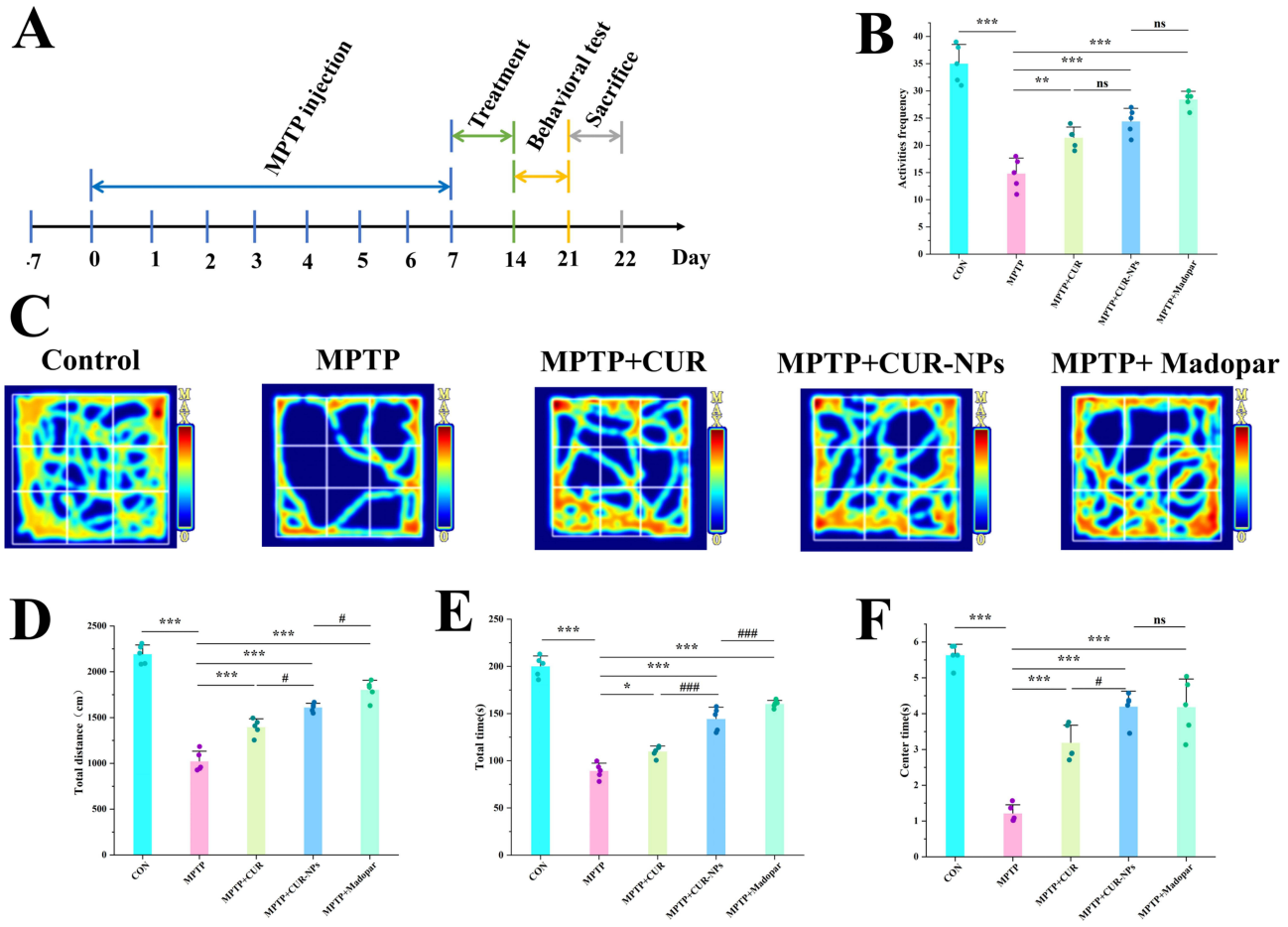

Figure 7 Effects of CUR-NPs on spontaneous activity and open field tests in MPTP-Induced PDModel Mice: (**A**) Flowchart of the MPTP-induced PD model and behavioral treatment experiments; (**B**) Quantitative analysis of spontaneous activity counts in PD mice; (**C**) Locomotor trajectories of mice from different groups in the open field test (MPTP-induced PD model); (**D** and **E**) Quantitative analysis of open field test results: (**D**) Total distance traveled, (**E**) Total movement time (**F**) Center time. n=5 sample size. Note:Control group refers to healthy mice treated with saline. Data are expressed as mean ± standard deviation (SD). *p < 0.05, **p < 0.01, ***p < 0.001 vs MPTP group. $^{\#}$p < 0.05, $^{\#\#\#}$p < 0.001 vs CUR-NPs group. ns: not significant.

16S rRNA Sequencing Analysis

Figure 13A reveals near-unity Good's coverage across all groups, suggesting adequate sequence depth and representative sampling. Shannon index results revealed the highest diversity index in the Control group, signifying optimal species richness and evenness. The Madopar and CUR-NPs groups showed intermediate diversity, while the MPTP group exhibited the lowest diversity. Non-metric multidimensional scaling (NMDS) analysis (Figure 13B) showed a Stress value < 0.2, indicating a good fit. The Control and MPTP groups differed significantly. The gut microbiota composition of the CUR-NPs group closely resembled that of the Control group, suggesting minimal impact on the microbiota. In contrast, the Madopar group differed considerably from the Control group, indicating a potentially significant impact on gut flora.

An elevated Firmicutes/Bacteroidetes (F/B) ratio is associated with enhanced neuroinflammatory responses and microglial activation. Phylum-level examination (Figure 13C) showcased substantial intergroup disparities in the F/B ratio, with the MPTP group displaying the most elevated ratio against the Control group. Post-treatment, CUR-NPs exhibited a notably reduced F/B ratio compared to MPTP, with Madopar displaying enhancement as well. Suggesting the F/B ratio may influence PD progression. Furthermore, Actinobacteria abundance changed significantly: the MPTP group exhibited a notable dip in abundance compared to the control group. However, treatment with CUR-NPs and Madopar brought those levels back up, nearly matching those of the control group. Zooming out to the class level, Bacteroidia were significantly more abundant in the control group than in the MPTP group. Conversely, the MPTP group showed

https://doi.org/10.2147/DDDT.S566113

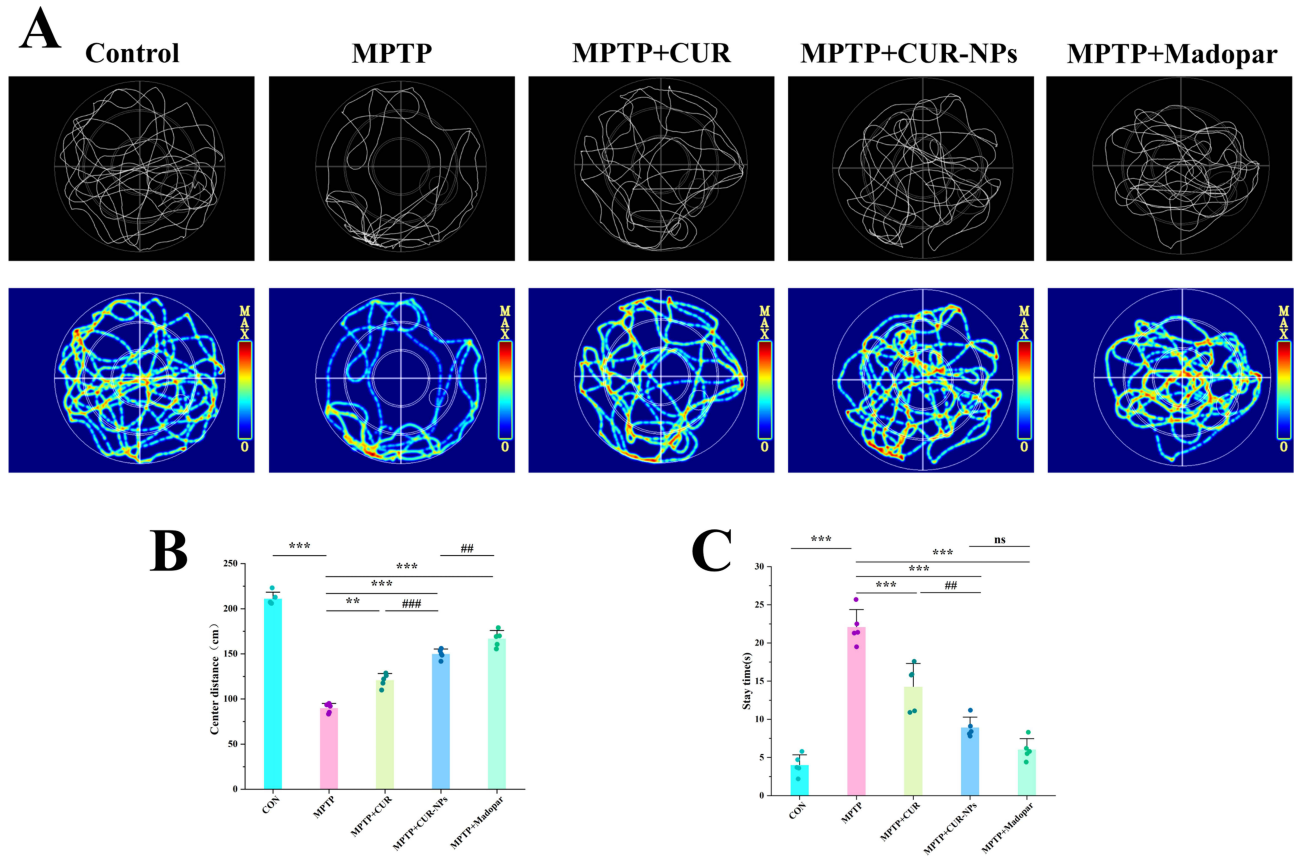

Figure 8 Effects of CUR nanoparticles on the Morris water maze test in MPTP-Induced PD Model: Mice (**A**) Swimming trajectories of PD mice in the Morris water maze test; (**B** and **C**) Quantitative analysis of Morris water maze results: (**B**) Platform crossing center distance, (**C**) Stay time. n=5 sample size. Data are expressed as mean ± standard deviation (SD). $^{**}p < 0.01$, $^{***}p < 0.001$ vs MPTP group. $^{\#\#}p < 0.01$, $^{\#\#\#\#}p < 0.001$ vs CUR-NPs group. ns: not significant.

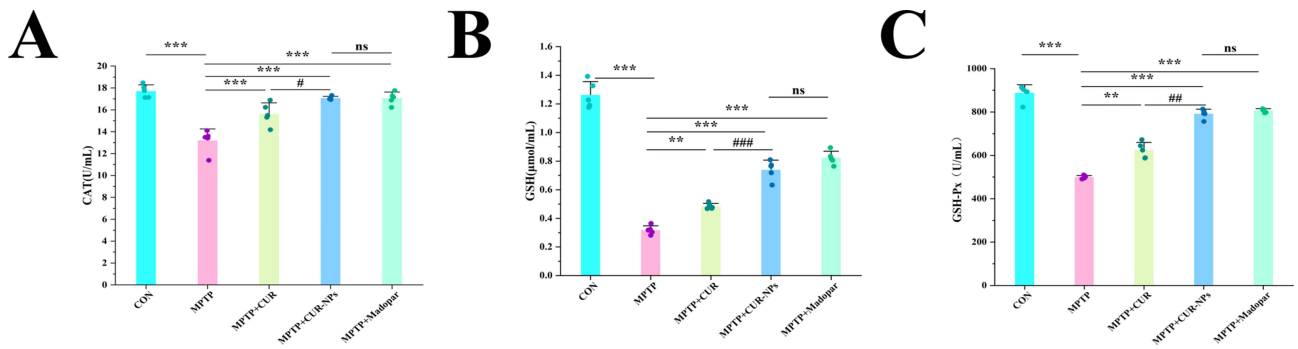

Figure 9 Effects of CUR-NPs on Antioxidant Stress in MPTP-Induced Parkinson's Disease Model: Mice (A-C) Quantitative results of antioxidant enzyme activity: (**A**) Catalase (CAT) activity, (**B**) Glutathione (GSH) level, (**C**) Glutathione peroxidase (GSH-Px) activity; n=5 sample size. Data are expressed as mean ± standard deviation (SD). $^{**}p < 0.01$, $^{***}p < 0.001$ vs MPTP group. $^{\#}p < 0.05$, $^{\#\#}p < 0.01$, $^{\#\#\#\#}p < 0.001$ vs CUR-NPs group. ns: not significant.

a significantly higher abundance of Bacilli and Actinobacteria classes when stacked up against the control group. This suggests a weakening of the protective effects usually offered by Lactobacillus and Bifidobacterium, potentially paving the way for the proliferation of Streptococcus and Corynebacterium. The gut microbiome in PD mice exhibited changes consistent with the disease state, concurrent with increased neuroinflammation. These changes included an expansion of pro-inflammatory taxa such as Burkholderiales. At the order level (Figure 13D), the MPTP group exhibited significantly higher abundances of Burkholderiales, Caulobacterales, Veillonellales-Selenomonadales, and Micrococcales compared to the CUR-NPs group.

https://doi.org/10.2147/DDDT.S566113

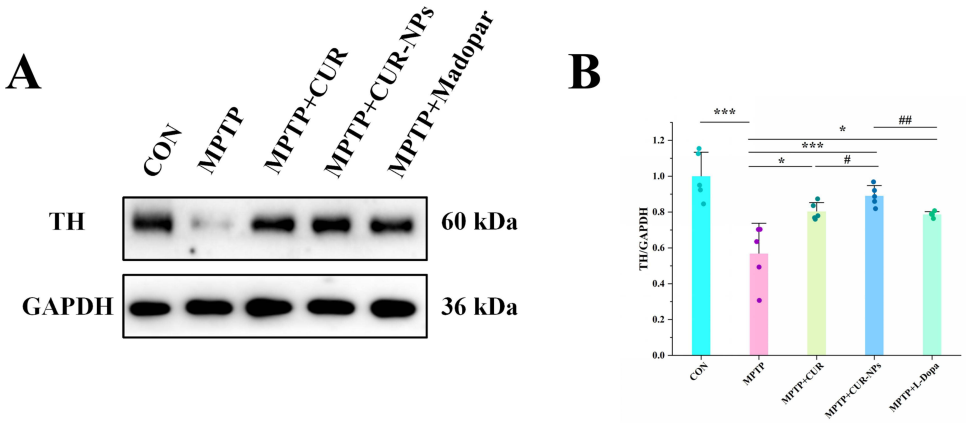

Figure 10 Effects of CUR-NPs on Neuroprotection in MPTP-Induced Parkinson's Disease Model: Mice (**A**) Expression of tyrosine hydroxylase (TH) protein in brain tissues of PD mice from different treatment groups detected by Western blotting; (**B**) Quantitative analysis of TH protein expression using glyceraldehyde-3-phosphate dehydrogenase (GAPDH) as the loading control. n=5 sample size. Data are expressed as mean ± standard deviation (SD). *p < 0.05, ***p < 0.001 vs MPTP group. #p < 0.05, ##p < 0.01 vs CUR-NPs group.

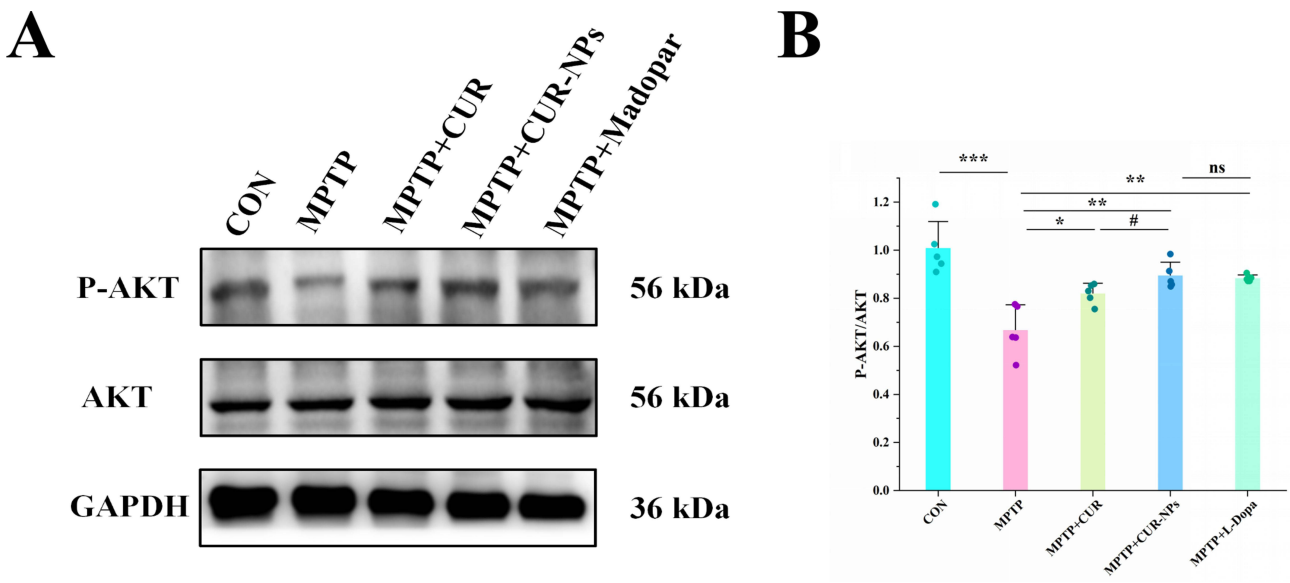

Figure 11 Effects of CUR nanoparticles on the expression of Akt pathway-related proteins in MPTP-induced Parkinson's disease model mice: (**A**) Expression of Akt signaling pathway-related proteins (P-AKT, AKT) in different treatment groups detected by Western blotting; (**B**) P-AKT/AKT ratio analysis;n=5 sample size. Data are expressed as mean ± standard deviation (SD). Data are expressed as mean ± standard deviation (SD). *p < 0.05, **p < 0.01, ***p < 0.001 vs MPTP group. #p < 0.05 vs CUR-NPs group. ns: not significant.

LEfSe (Linear Discriminant Analysis effect size) methodology (Figure 14A) contrasted CUR-NPs and Madopar's effects on gut microbiota structure. The CUR-NPs group showed higher absolute LDA scores, indicating significant structural differences between the groups. The CUR-NPs group exhibited prominent enrichment of probiotics (eg, Lactobacillus), while the Madopar group showed dominance in genera such as Caulobacter, Comamonadaceae, Leptotrichiaceae, Streptococcus, and Eubacterium (some of which are conditional pathogens or inflammation-associated).

Metabolic pathway analysis (Figure 14B) revealed that the control group had a distinct leg up on the MPTP group when it came to pathways involved in churning out and processing carbs, generating energy, handling amino acids, and dealing with cofactors and vitamins. They simply blew the MPTP group out of the water in these areas. Conversely, the MPTP group showed higher enrichment in membrane transport and enzyme-related metabolic pathways. When you stack up the CUR-NP group against the MPTP group, the MPTP group really shows a marked increase in protein metabolism,

https://doi.org/10.2147/DDDT.S566113

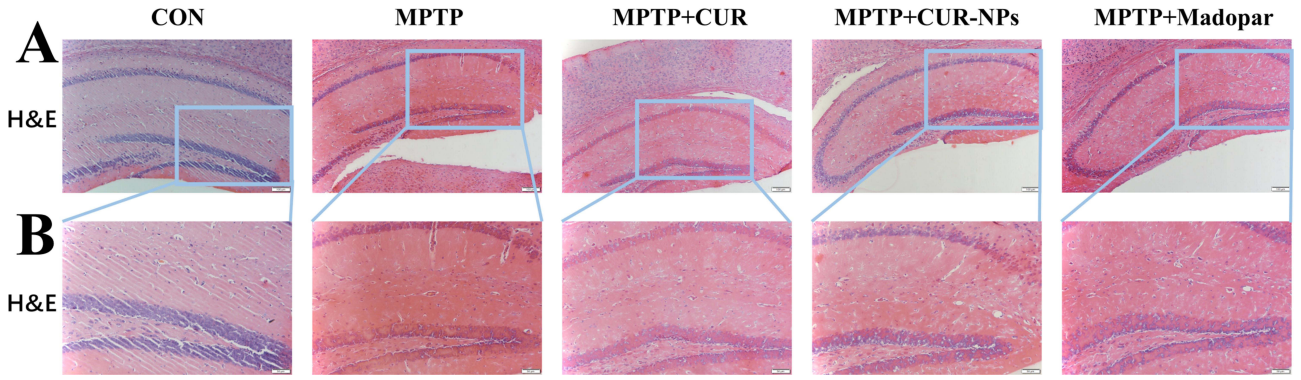

Figure 12 Hematoxylin and eosin (H&E) staining showing pathological changes in the dentate gyrus (DG) region of brain tissues from PD mice in different treatment groups: (**A**) 100x (**B**) 200x. The blue square box highlights the area shown at higher magnification in panel.

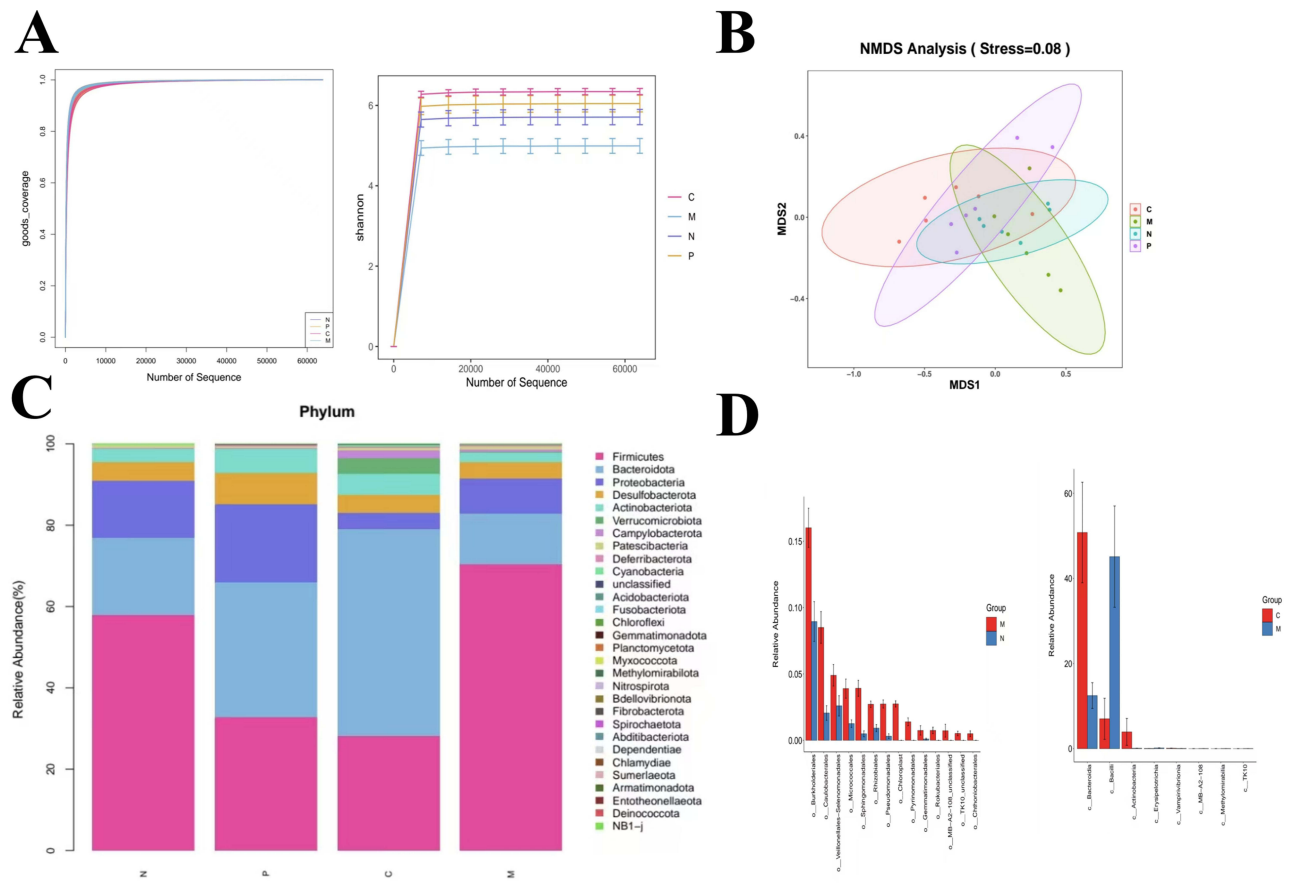

Figure 13 Analysis of the Effects of CUR-NPs on Gut Microbiota in MPTP-Induced Parkinson's Disease Mice via 16S rRNA Sequencing (n = 6): (**A**) Analysis of sequencing depth and Shannon index of gut microbiota in the four sample groups; (**B**) Non-metric multidimensional scaling (NMDS) analysis of the four sample groups; (**C**) Phylum-level relative abundance bar plot analysis of gut microbiota; (**D**) Class-level relative abundance analysis (comparing Blank group vs MPTP group) and Order-level relative abundance bar plot analysis (comparing MPTP group vs CUR-NPs group). Submitted samples included: Control group (Group C), MPTP group (Group M), MPTP combined with CUR-NPs group (N), and MPTP combined with Madopar group (Group P).

specifically when it comes to proteins linked to K09165 (uncharacterized protein), plus phaz, ctaE, chpB, PilJ, murU, imuA, amgK, and shc. These proteins are implicated in energy metabolism, neuroinflammation, DNA repair, and oxidative stress responses. Metabolic profiling indicated that the counts of facultative anaerobes (Figure 14C) were notably increased in the MPTP group relative to the Control group; CUR-NPs treatment significantly reduced this abundance.

https://doi.org/10.2147/DDDT.S566113

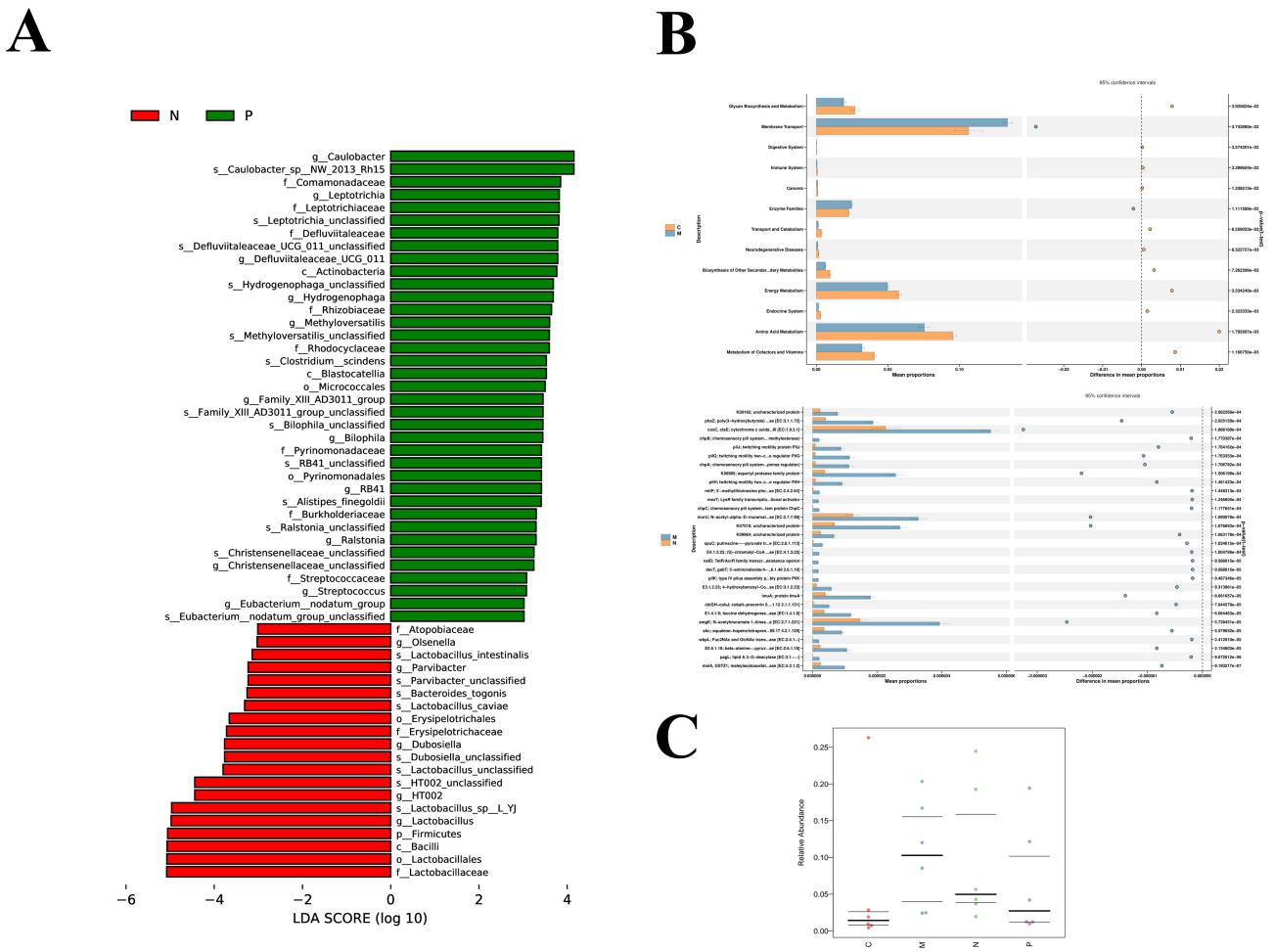

Figure 14 Effects of CUR-NPs on LDA and metabolism in an MPTP-induced Parkinson's disease model via 16S rRNA Sequencing (n=6): (**A**) Linear discriminant analysis (LDA) results for gut microbiota comparing the CUR-NPs group vs Madopar group; (**B**) Gut microbiota metabolic function analysis comparing differences among the Blank group vs MPTP group and the MPTP group vs CUR-NPs group; (**C**) Analysis of facultative anaerobe abundance in the four sample groups. Submitted samples included: Control group (Group C), MPTP group (Group M), MPTP combined with CUR-NPs group (N), and MPTP combined with Madopar group (Group P).

Discussion

Parkinson's disease, a neurodegenerative disorder characterized by the progressive loss of dopaminergic neurons, poses an increasingly severe public health burden amidst the accelerating global aging trend. Current pharmacological treatments, such as levodopa, provide temporary symptomatic relief, but their efficacy wanes with disease progression and is often accompanied by motor complications and other side effects.[21] This clinical challenge underscores the urgent need for novel therapeutic strategies capable of multi-target intervention. In this study, we developed a curcumin nano-formulation (CUR-NPs) that demonstrated significant efficacy in an MPTP-induced Parkinson's disease model. Its mechanism of action potentially involves the activation of the Akt signaling pathway, alleviation of oxidative stress, and remodeling of the gut microbiota.((Figure 15).

The clinical application of curcumin is severely limited by its inherently low bioavailability.[22–24] Despite possessing excellent antioxidant and anti-inflammatory properties,[25] its poor aqueous solubility and rapid systemic metabolism impede the full realization of its neuroprotective potential. The nano-delivery system constructed using an mPEG-PLGA carrier in this study effectively enhanced the solubility and stability of curcumin. The superior therapeutic efficacy of CUR-NPs over free curcumin can be attributed to the improved bioavailability and enhanced solubility conferred by the mPEG-PLGA nanocarrier, a finding consistent with previous research,[26] and corroborated by our results showing better outcomes in behavioral tests and Western blot analyses for the CUR-NPs group. Compared to other curcumin nano-formulations,[27–29] our CUR-NPs exhibited significant advantages in improving motor function and potentially increasing

https://doi.org/10.2147/DDDT.S566113

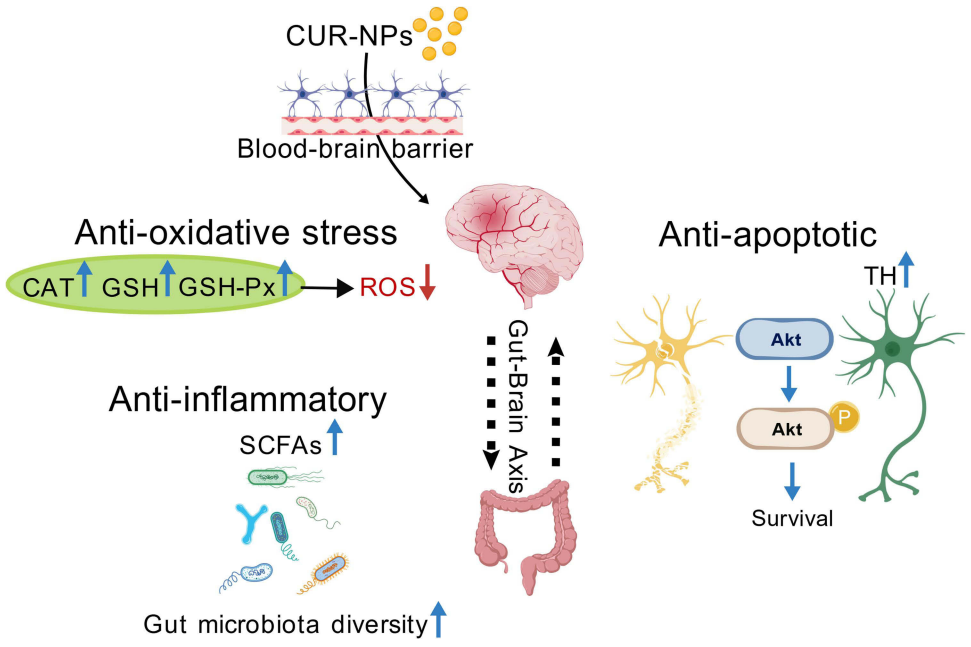

Figure 15 Schematic diagram of the therapeutic mechanism of CUR-NPs against Parkinson's disease. Upward and downward arrows indicate increase and decrease, respectively. (Created with BioGDP.com).

drug concentration in the brain, aligning with recent studies on nanocarriers enhancing blood-brain barrier penetration.[30] Notably, the excellent performance of CUR-NPs in behavioral tests was highly consistent with their effects at the molecular level, confirming the critical value of nanotechnology in overcoming the challenges of poor solubility and low bioavailability.

Network pharmacology analysis identified eight core targets. A comprehensive evaluation using multiple algorithms within cytoHubba indicated that AKT1 consistently achieved the highest score among them, leading to its selection for subsequent experimental validation. Molecular docking revealed a strong binding affinity between curcumin and AKT1 (−6.3 kcal/mol). Molecular dynamics simulations further confirmed the stability of the complex over a 100 ns simulation, with the number of hydrogen bonds maintained at approximately three. Our Western blot results demonstrated that CUR-NPs significantly increased the p-AKT/AKT ratio and tyrosine hydroxylase expression. This finding strongly aligns with the current understanding of the central role of the Akt pathway in neuroprotection.[31–33]

H&E staining of the hippocampal dentate gyrus region revealed marked neuronal loss, disorganized arrangement, and nuclear pyknosis in the MPTP model group, pathological features consistent with previously reported MPTP neurotoxicity.[34,35] In contrast, CUR-NPs treatment significantly ameliorated neuronal morphology, increased neuronal density, and restored normal cellular architecture. These histological findings not only confirm the protective effect of CUR-NPs on dopaminergic neurons but also correlate well with our Western blot observations of upregulated TH expression and Akt pathway activation, collectively building a verification chain from the molecular to the cellular level.

The role of gut microbiota in the pathogenesis of Parkinson's disease is gaining increasing attention.[36–38] Our 16S rRNA sequencing results showed that CUR-NPs significantly restored the gut microbiota dysbiosis induced by MPTP, reduced the elevated Firmicutes/Bacteroidetes ratio, and promoted the proliferation of beneficial bacteria such as *Lactobacillus*. These microbiome findings relate to recent studies; Hassan et al confirmed that *Lactobacillus* can restore dopamine synthesis and alleviate neuroinflammation,[39] while Qu et al revealed a new mechanism whereby short-chain fatty acids modulate α-synuclein aggregation via the GPR43-NLRP3 signaling pathway.[40] Particularly noteworthy is the positive correlation observed in our results between the improvement in gut microbiota induced by CUR-NPs and the enhancement of serum antioxidant stress-related indicators, suggesting an important role for the "gut microbiota-oxidative stress" axis in Parkinson's disease.

The metabolic analysis of the gut microbiota aligns with recent research on metabolic abnormalities in Parkinson's disease.[41,42] Our metabolic pathway analysis revealed significant downregulation in multiple key pathways in the MPTP model group, including carbohydrate metabolism, energy metabolism, and amino acid metabolism, which were effectively reversed by CUR-NPs treatment. It is especially notable that the upregulation of proteins associated with neuroinflammation (eg, PilJ, murU) and oxidative stress (eg, chpB, imuA) in the MPTP group was significantly suppressed following CUR-NPs intervention.

This study has several limitations. First, while the acute MPTP model is widely used,[43,44,45] its pathological process differs from the chronic progression of human Parkinson's disease. Future studies employing genetic models such as A53T could help validate the current findings in a context more closely resembling clinical pathology. Second, the direct causal link between gut microbiota changes and the central protective effects still requires further verification through experiments like fecal microbiota transplantation.

In conclusion, this study, through an integrated strategy, systematically elucidates the mechanism by which CUR-NPs exert therapeutic effects against Parkinson's disease by modulating the Akt signaling pathway and the gut microbiota. Our work not only provides a theoretical basis for the clinical application of curcumin but also opens new avenues for developing nanotherapeutic strategies based on natural products. As understanding of neurodegenerative disease mechanisms deepens, this research paradigm, which integrates nanotechnology, computational biology, and experimental validation, holds promise for bringing new breakthroughs in the treatment of complex diseases.

Conclusion

This study developed CUR-NPs, which significantly ameliorated motor dysfunction, attenuated oxidative stress, and reduced dopaminergic neuron damage in MPTP-induced Parkinson's disease mice. The study further revealed that the neuroprotective effects of CUR-NPs are likely mediated through activation of the Akt signaling pathway and remodeling of the gut microbiota. This work not only presents a promising nano-drug candidate for Parkinson's disease treatment but also validates the feasibility of a multi-target therapeutic strategy utilizing natural products for managing complex diseases.

Abbreviations

AKT, protein kinase B; CUR, Curcumin; CUR-NPs, Curcumin-loaded nanoparticles; CAT, Catalase; GO, Gene Ontology; GAPDH, glyceraldehyde 3-phosphate dehydrogenase; GSH-Px, Glutathione peroxidase; GSH, Glutathione; H&E, Hematoxylin and Eosin; MPTP,1-Methyl-4-Phenyl-1,2,3,6-Tetrahydropyridine;MD simulations, Molecular Dynamics simulations; PPI, Protein-Protein interaction; PD, Parkinson's disease; PI3K, Phosphatidylinositol-3-kinase; RMSD, Root mean square deviation; RMSF, Root mean square fluctuation; Rg, Radius of gyration; SASA, Solvent-accessible surface area; TCM, Traditional Chinese Medicine; TH, tyrosine hydroxylase; and, WHO, World Health Organization.

Ethical Approval

Ethical clearance for this investigation was formally granted during August 2024 by the Laboratory Animal Ethics Committee at Beihua University (Approval No. 2024082117). Animal welfare adheres to the American Veterinary Medical Association (AVMA) Animal Welfare Principles.

Author Contributions

All authors made a significant contribution to the work reported, whether that is in the conception, study design, execution, acquisition of data, analysis and interpretation, or in all these areas; took part in drafting, revising or critically reviewing the article; gave final approval of the version to be published; have agreed on the journal to which the article has been submitted; and agree to be accountable for all aspects of the work.

Funding

This work was supported by the Jilin Science and Technology Development Programme Project, China (YDZJ202401432ZYTS), and also supported by the Jilin Science and Technology Development Programme Project, China (No. 20210204158YY).

Disclosure

The authors declare that there are no conflicts of interest in this work.

References

1. Zhang J, Fan Y, Liang H, Zhang Y. Global, regional and national temporal trends in Parkinson's disease incidence, disability-adjusted life year rates in middle-aged and older adults: a cross-national inequality analysis and Bayesian age-period-group analysis based on the global burden of disease 2021. *Neurol Sci*. 2025;46(4):1647–1660. doi:10.1007/s10072-024-07941-7
2. Bloem BR, Okun MS, Klein C. Parkinson's disease. *Lancet*. 2021;397(10291):2284–2303. doi:10.1016/S0140-6736(21)00218-X
3. Kwon DK, Kwatra M, Wang J, Ko HS. Levodopa-induced dyskinesia in parkinson's disease: pathogenesis and emerging treatment strategies. *Cells*. 2022;11(23):3736. doi:10.3390/cells11233736
4. Sun J, Qi X, Yang C, et al. Network pharmacology, molecular docking, and in vitro experiments reveal the role and mechanism of tanshinone iia in colorectal cancer treatment through the PI3K/AKT pathway. *Drug Des Devel Ther*. 2025;19:2959–2977. doi:10.2147/DDDT.S492033
5. Cai B, Qi M, Zhang X, Zhang D. Integrating network pharmacology with in vitro experiments to validate the efficacy of celastrol against hepatocellular carcinoma through ferroptosis. *Drug Des Devel Ther*. 2024;18:3121–3141. doi:10.2147/DDDT.S450324
6. Li R, Wang Y, Lao Y, et al. Effect and mechanism of aloin in ameliorating chronic prostatitis/chronic pelvic pain syndrome: network pharmacology and experimental verification. *Drug Des Devel Ther*. 2025;19:1945–1969. doi:10.2147/DDDT.S473678
7. Abd El-Hack ME, El-Saadony MT, Swelum AA, et al. Curcumin, the active substance of turmeric: its effects on health and ways to improve its bioavailability. *J Sci Food Agric*. 2021;101(14):5747–5762. doi:10.1002/jsfa.11372
8. Fernández-Lázaro D, Mielgo-Ayuso J, Seco Calvo J, Córdova Martínez A, Caballero García A, Fernandez-Lazaro CI. Modulation of exercise-induced muscle damage. Inflammation, and Oxidative Markers by Curcumin Supplementation in a Physically Active Population. *Nutrients*. 2020;12(2):501. doi:10.3390/nu12020501
9. Timmons S, Coakley MF, Moloney AM, Neill O. Akt signal transduction dysfunction in Parkinson's disease. *Neurosci Lett*. 2009;467(1):30–35. doi:10.1016/j.neulet.2009.09.055
10. Zhang P, Zhang D, Zhou W, et al. Network pharmacology: towards the artificial intelligence-based precision traditional Chinese medicine. *Brief Bioinform*. 2023;25(1):bbad518. doi:10.1093/bib/bbad518
11. Li S, Cai Y, Wang S, et al. Gut microbiota: the indispensable player in neurodegenerative diseases. *J Sci Food Agric*. 2024;104(12):7096–7108. doi:10.1002/jsfa.13509
12. Mou Y, Du Y, Zhou L, et al. Gut microbiota interact with the brain through systemic chronic inflammation: implications on neuroinflammation, neurodegeneration, and aging. *Front Immunol*. 2022;13:796288. doi:10.3389/fimmu.2022.796288
13. Warnecke T, Schäfer KH, Claus I, Del Tredici K, Jost WH. Gastrointestinal involvement in Parkinson's disease: pathophysiology, diagnosis, and management. *NPJ Parkinsons Dis*. 2022;8(1):31. doi:10.1038/s41531-022-00295-x
14. Zhu M, Liu X, Ye Y, et al. Gut microbiota: a novel therapeutic target for parkinson's disease. *Front Immunol*. 2022;13:937555. doi:10.3389/fimmu.2022.937555
15. Scheperjans F, Aho V, Pereira PA, et al. Gut microbiota are related to Parkinson's disease and clinical phenotype. *Mov Disord*. 2015;30(3):350–358. doi:10.1002/mds.26069
16. Lagoa R, Rajan L, Violante C, et al. Application of curcuminoids in inflammatory, neurodegenerative and aging conditions - Pharmacological potential and bioengineering approaches to improve efficiency. *Biotechnol Adv*. 2025;82:108568. doi:10.1016/j.biotechadv.2025.108568
17. Lin SP, Zhu L, Shi H, et al. Puerarin prevents sepsis-associated encephalopathy by regulating the AKT1 pathway in microglia. *Phytomedicine*. 2023;121:155119. doi:10.1016/j.phymed.2023.155119
18. Elfil M, Kamel S, Kandil M, Koo BB, Schaefer SM. Implications of the gut microbiome in parkinson's disease. *Mov Disord*. 2020;35(6):921–933. doi:10.1002/mds.28004
19. Wang Q, Luo Y, Ray Chaudhuri K, Reynolds R, Tan EK, Pettersson S. The role of gut dysbiosis in Parkinson's disease: mechanistic insights and therapeutic options. *Brain*. 2021;144(9):2571–2593. doi:10.1093/brain/awab156
20. Boyton I, Valenzuela SM, Collins-Praino LE, Care A. Neuronanomedicine for alzheimer's and parkinson's disease: current progress and a guide to improve clinical translation. *Brain, Behav Immun*. 2024;115:631–651. doi:10.1016/j.bbi.2023.11.004
21. Riederer P, Strobel S, Nagatsu T, et al. Levodopa treatment: impacts and mechanisms throughout Parkinson's disease progression. *J Neural Transm*. 2025;132(6):743–779. doi:10.1007/s00702-025-02893-4
22. Toden S, Goel A. the holy grail of curcumin and its efficacy in various diseases: is bioavailability truly a big concern ? *J Restor Med*. 2017;6(1):27–36. doi:10.14200/jrm.2017.6.0101
23. Urošević M, Nikolić L, Gajić I, Nikolić V, Dinić A, Miljković V. Curcumin: biological activities and modern pharmaceutical forms. *Antibiotics*. 2022;11(2):135. doi:10.3390/antibiotics11020135
24. Liu S, Liu J, He L, et al. A comprehensive review on the benefits and problems of curcumin with respect to human health. *Molecules*. 2022;27(14):4400. doi:10.3390/molecules27144400
25. Benameur T, Giacomucci G, Panaro MA, et al. New promising therapeutic avenues of curcumin in brain diseases. *Molecules*. 2021;27(1):236. doi:10.3390/molecules27010236
26. Chen X, Wang D, Guo X, et al. Curcumin-Loaded mPEG-PLGA nanoparticles attenuates the apoptosis and corticosteroid resistance induced by cigarette smoke extract. *Front Pharmacol*. 2022;13:824652. doi:10.3389/fphar.2022.824652
27. Józsa L, Vasvári G, Sinka D, et al. Enhanced antioxidant and anti-inflammatory effects of self-nano and microemulsifying drug delivery systems containing curcumin. *Molecules*. 2022;27(19):6652. doi:10.3390/molecules27196652
28. Yang C, Han M, Li R, et al. Curcumin nanoparticles inhibiting ferroptosis for the enhanced treatment of intracerebral hemorrhage. *Int J Nanomed*. 2021;16:8049–8065. doi:10.2147/IJN.S334965
29. Guo X, Qiao X, Li X, et al. Lactoferrin-modified organic-inorganic hybrid mesoporous silica for co-delivery of levodopa and curcumin in the synergistic treatment of Parkinson's disease. *Phytomedicine*. 2025;140:156547. doi:10.1016/j.phymed.2025.156547

30. Du Q, Liu Y, Fan M, Wei S, Ismail M, Zheng M. PEG length effect of peptide-functional liposome for blood brain barrier (BBB) penetration and brain targeting. *J Control Release*. 2024;372:85–94. doi:10.1016/j.jconrel.2024.06.005
31. Aleyasin H, Rousseaux MW, Marcogliese PC, et al. DJ-1 protects the nigrostriatal axis from the neurotoxin MPTP by modulation of the AKT pathway. *Proc Natl Acad Sci U S A*. 2010;107(7):3186–3191. doi:10.1073/pnas.0914876107
32. Ali MZ, Dholaniya PS. Oxidative phosphorylation mediated pathogenesis of Parkinson's disease and its implication via Akt signaling. *Neurochem Int*. 2022;157:105344. doi:10.1016/j.neuint.2022.105344
33. Zhang X, Xu S, Hu Y, et al. Irisin exhibits neuroprotection by preventing mitochondrial damage in Parkinson's disease. *NPJ Parkinsons Dis*. 2023;9(1):13. doi:10.1038/s41531-023-00453-9
34. Meng X, Lin S, Zhu M, et al. Ultrasound-assisted enzyme extraction of Citri Exocarpium Rubrum (Juhong) polysaccharides and its structural characteristics and evaluation of improving Parkinson's disease through HDAC6/NLRP3 pathway. *Ultrason Sonochem*. 2025;122:107636. doi:10.1016/j.ultsonch.2025.107636
35. Lv M, Duan Z, Tan J, et al. PHGDH-mediated serine synthesis in astrocytes supports neuroinflammation by sustaining NADH level to promote histone acetylation. *Cell Death Dis*. 2025;16(1):397. doi:10.1038/s41419-025-07732-8
36. Khalil M, Di Ciaula A, Mahdi L, et al. Unraveling the role of the human gut microbiome in health and diseases. *Microorganisms*. 2024;12 (11):2333. doi:10.3390/microorganisms12112333
37. Braak H, Del Tredici K, Rüb U, et al. Staging of brain pathology related to sporadic Parkinson's disease. *Neurobiol Aging*. 2003;24(2):197–211. doi:10.1016/s0197-4580(02)00065-9
38. Wu J, Li CS, Huang WY, et al. Gut microbiota promote the propagation of pathologic α-syn from gut to brain in a gut-originated mouse model of Parkinson's disease. *Brain Behav Immun*. 2025;128:152–169. doi:10.1016/j.bbi.2025.04.001
39. Hassan HM, Abou-Hany HO, Shata A, et al. Vinpocetine and lactobacillus attenuated rotenone-induced parkinson's disease and restored dopamine synthesis in rats through modulation of oxidative stress, neuroinflammation, and lewy bodies inclusion. *J Neuroimmune Pharmacol*. 2025;20(1):22. doi:10.1007/s11481-025-10176-8
40. Qu Y, An K, Wang D, et al. Short-chain fatty acid aggregates alpha-synuclein accumulation and neuroinflammation via GPR43-NLRP3 signaling pathway in a model parkinson's disease. *Mol Neurobiol*. 2025;62(5):6612–6625. doi:10.1007/s12035-025-04726-7
41. Li H, Zeng F, Huang C, et al. The potential role of glucose metabolism, lipid metabolism, and amino acid metabolism in the treatment of Parkinson's disease. *CNS Neurosci Ther*. 2024;30(2):e14411. doi:10.1111/cns.14411
42. Chen L, Wang C, Qin L, Zhang H. Parkinson's disease and glucose metabolism impairment. *Transl Neurodegener*. 2025;14(1):10. doi:10.1186/s40035-025-00467-8
43. Mustapha M, Mat Taib CN. MPTP-induced mouse model of Parkinson's disease: a promising direction of therapeutic strategies. *Bosn J Basic Med Sci*. 2021;21(4):422–433. doi:10.17305/bjbms.2020.5181
44. Yildirim S, Ozkan A, Aytac G, Agar A, Tanriover G. Role of melatonin in TLR4-mediated inflammatory pathway in the MTPT-induced mouse model. *Neurotoxicology*. 2022;88:168–177. doi:10.1016/j.neuro.2021.11.011
45. Xu K, Huang P, Wu Y, et al. Engineered selenium/human serum albumin nanoparticles for efficient targeted treatment of parkinson's disease via oral gavage. *ACS Nano*. 2023;17(20):19961–19980. doi:10.1021/acsnano.3c05011